Article

Tunable Inhibition and Denaturation of α-Chymotrypsin with Amino Acid-Functionalized Gold Nanoparticles

Chang-Cheng You, Mrinmoy De, Gang Han, and Vincent M. Rotello

J. Am. Chem. Soc., **2005**, 127 (37), 12873-12881• DOI: 10.1021/ja0512881 • Publication Date (Web): 23 August 2005

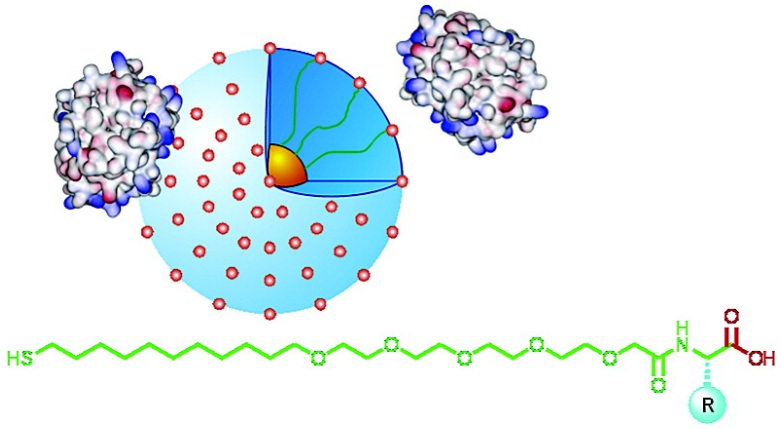

More About This Article

Additional resources and features associated with this article are available within the HTML version:

- Supporting Information
- Links to the 21 articles that cite this article, as of the time of this article download
- Access to high resolution figures
- Links to articles and content related to this article
- Copyright permission to reproduce figures and/or text from this article

View the Full Text HTML

J|A|C|S
ARTICLES
Published on Web 08/23/2005

Tunable Inhibition and Denaturation of α-Chymotrypsin with Amino Acid-Functionalized Gold Nanoparticles

Chang-Cheng You, Mrinmoy De, Gang Han, and Vincent M. Rotello*

Contribution from the Department of Chemistry, University of Massachusetts, 710 North Pleasant Street, Amherst, Massachusetts 01003

Received March 1, 2005; E-mail: rotello@chem.umass.edu

Abstract: Water-soluble gold nanoparticles bearing diverse L-amino acid terminals have been fabricated to probe the effect of receptor surface on protein surface binding. The interaction of these nanoparticles with α-chymotrypsin (ChT) was investigated by activity assay, gel electrophoresis, zeta-potential, circular dichroism, and fluorescence spectroscopy. The results show that both electrostatic and hydrophobic interactions between the hydrophobic patches of receptors and the protein contribute to the stability of the complex. The microscopic binding constants for these receptor−protein systems are 10^6-10^7 M^{-1}, with the capacity of the nanoparticle receptors to bind proteins determined by both their surface area and their surface charge density. Furthermore, it is found that the hydrophilic side chains destabilize the ChT structure through either competitive hydrogen bonding or breakage of salt bridges, whereas denaturation was much slower with hydrophobic amino acid side chains. Significantly, correlation between the hydrophobicity index of amino acid side chains and the binding affinity and denaturation rates was observed.

Introduction

Protein surface recognition is an important issue in biomedical and biomaterial research.[1] Surface recognition provides a method complementary to active site inhibition for the control of enzymatic processes.[2] More significantly, protein surface recognition provides a powerful tool for the regulation of protein−protein interactions central to a number of cellular processes, such as cellular signal transduction, DNA transcription, and protein antigen/antibody recognition.[3,4] Protein surface recognition is an important issue in biosensing, in clinical diagnostics, and in pharmacology. For example, interruption of protein−protein interactions has been used by Chmielewski to inhibit the dimerization and hence activity of HIV-1 protease[5] and Burgess to disrupt NGF−TrkA binding.[6]

The required large receptor−protein contact areas[7] (usually >6 nm^2) and the inherent complexity of protein surfaces, such as multiple electrostatic, hydrophobic and hydrogen-bonding interactions, and complicated topological features,[8] must be addressed to attain specific protein surface recognition. A few "small molecule" systems, such as the receptors on calixarene and porphyrin scaffolds,[9] cyclodextrin dimers,[10] and transition metal complexes targeted against surface exposed histidines,[11] have been recently fabricated to address the challenge for protein surface recognition and have shown the ability to modulate the structure and function of biomolecules.

The use of scaffolds with large surface is advantageous, however, as such receptors could offer larger area of contact for efficient molecular recognition. In this regard, monolayer-protected clusters (MPCs) and mixed monolayer-protected clusters (MMPCs) are promising candidates that provide many desirable structural attributes for the creation of biomacromolecular receptors. First, a variety of metal and semiconductor core materials that feature useful fluorescence and magnetic properties can be used to construct the nanoparticle scaffolds.[12] Second, the core sizes of nanoparticles are tunable from 2 to

(1) Fairlie, D. P.; West, M. L.; Wong, A. K. *Curr. Med. Chem.* **1998**, *5*, 29−62.
(2) Peczuh, M. W.; Hamilton, A. D. *Chem. Rev.* **2000**, *100*, 2479−2493.
(3) Branden, C.; Tooze, J. *Introduction to Protein Structure*, 2nd ed.; Garland: New York, 1999.
(4) (a) Gadek, T. R.; Nicholas, J. B. *Biochem. Parmacol.* **2003**, *65*, 1−8. (b) Toogood, P. L. *J. Med. Chem.* **2002**, *45*, 1543−1558.
(5) (a) Shultz, M. D.; Ham, Y. W.; Lee, S. G.; Davis, D. A.; Brown, C.; Chmielewski, J. *J. Am. Chem. Soc.* **2004**, *126*, 9886−9887. (b) Shultz, M. D.; Chmielewski, J. *Bioorg. Med. Chem. Lett.* **1999**, *9*, 2431−2436. (c) Zutshi, R.; Franciskovich, J.; Shultz, M.; Schweitzer, B.; Bishop, P.; Wilson, M.; Chmielewski, J. *J. Am. Chem. Soc.* **1997**, *119*, 4841−4845.
(6) Burgess, K. *Acc. Chem. Res.* **2001**, *34*, 826−835.
(7) (a) Conte, L. L.; Chothia, C.; Janin, J. *J. Mol. Biol.* **1999**, *285*, 2177−2198. (b) Stites, W. E. *Chem. Rev.* **1997**, *97*, 1233−1250. (c) Jones, S.; Thornton, J. M. *Proc. Natl. Acad. Sci. U.S.A.* **1996**, *93*, 13−20.
(8) (a) Bogan, A. A.; Thorn, K. S. *J. Mol. Biol.* **1998**, *280*, 1−9. (b) Lijnzaad, P.; Argos, P. *Proteins* **1997**, *28*, 333−343.
(9) (a) Groves, K.; Wilson, A. J.; Hamilton, A. D. *J. Am. Chem. Soc.* **2004**, *126*, 12833−12842. (b) Wilson, A. J.; Groves, K.; Jain, R. K.; Park, H. S.; Hamilton, A. D. *J. Am. Chem. Soc.* **2003**, *125*, 4420−4421. (c) Ernst, J. T.; Becerril, J.; Park, H. S.; Yin, H.; Hamilton, A. D. *Angew. Chem., Int. Ed.* **2003**, *42*, 535−539. (d) Park, H. S.; Lin, Q.; Hamilton, A. D. *J. Am. Chem. Soc.* **1999**, *121*, 8−13. (e) Hamuro, Y.; Calama, M. C.; Park, H. S.; Hamilton, A. D. *Angew. Chem., Int. Ed. Engl.* **1997**, *36*, 2680−2683.
(10) Leung, D. K.; Yang, Z. W.; Breslow, R. *Proc. Natl. Acad. Sci. U.S.A.* **2000**, *97*, 5050−5053.
(11) Fazal, M. A.; Roy, B. C.; Sun, S. G.; Mallik, S.; Rodgers, K. R. *J. Am. Chem. Soc.* **2001**, *123*, 6283−6290.
(12) (a) Li, Z.; Sun, Q.; Gao, M. *Angew. Chem., Int. Ed.* **2005**, *44*, 123−126. (b) Lu, X.; Yu, Y.; Chen, L.; Mao, H.; Zhang, W.; Wei, Y. *Chem. Commun.* **2004**, 1522−1523. (c) Redl, F. X.; Black, C. T.; Papaefthymoiu, G. C.; Sandstrom, R. L.; Yin, M.; Zeng, H.; Murray, C. B.; O'Brien, S. P. *J. Am. Chem. Soc.* **2004**, *126*, 14583−14599. (d) Hu, J.; Zhang, Y.; Liu, B.; Liu, J.; Zhou, H.; Xu, Y.; Jiang, Y.; Yang, Z.; Tian, Z.-Q. *J. Am. Chem. Soc.* **2004**, *126*, 9470−9471. (e) Skaff, H.; Sill, K.; Emrick, T. *J. Am. Chem. Soc.* **2004**, *126*, 11322−11325. (f) Turro, N. J.; Lakshminarasimhan, P. H.; Jockusch, S.; O'Brien, S. P.; Grancharov, S. G.; Redl, F. X. *Nano Lett.* **2002**, *2*, 325−328.

>10 nm, which is comparable to that of proteins and other biomacromolecules, with concomitant large surface areas for efficient protein binding.[13] Third, the surface properties of nanoparticles can be conveniently tailored by appropriate selection of ligand functionality, providing versatility in the creation of surface-specific receptors.[14] Indeed, MPCs and MMPCs have shown interesting application in the multivalent binding of biomacromolecular targets.[15,16]

α-Chymotrypsin (ChT), a serine protease of 25 kDa, provides an excellent system for studying the protein surface recognition as it is an extensively characterized protein with well-defined geometry, surface "hot spot", and enzymatic activity. Our previous investigations have demonstrated that simple carboxylic acid-terminated nanoparticles (with either Au or CdSe core) could target ChT through complementary electrostatic interactions, resulting in the inhibition of ChT activity.[17] However, to allow more pragmatic uses of nanoparticles for regulation of protein−protein interaction, a prerequisite is the modification of the nanoparticle surface to better mimic protein surface functionality. This complexity would provide control over protein specificity and protein stability, giving insight into issues important in modulating protein−protein interactions such as complementary electrostatic interaction, hydrophobic interaction, and steric effect. Furthermore, through these studies we would be able to address other crucial issues, such as the factors contributing to stabilization/denaturation of MMPC-bound proteins.

Amino acids provide an attractive means for generating structural diversity.[18] In the current study, we have fabricated a series of L-amino acids-functionalized gold nanoparticles and examined their interaction with ChT (Figure 1). The amino acid-decorated surfaces represent the simplest mimics of protein surfaces. Their interaction with proteins thus exhibits much more resemblance with the naturally occurring protein−protein systems. In this study, we have found that the interactions between ChT and these MMPCs depend on the surface composition of nanoparticles. Significantly, the binding affinity as well as the stability of the protein is regulated by the charge and the hydrophobicity of amino acid side chains in the nanoparticles. Therefore, it is possible to control the association/dissociation and stabilization/denaturation of the protein at the MMPC interfaces through variation of the extra functionality in the vicinity of carboxylic acid recognition elements.

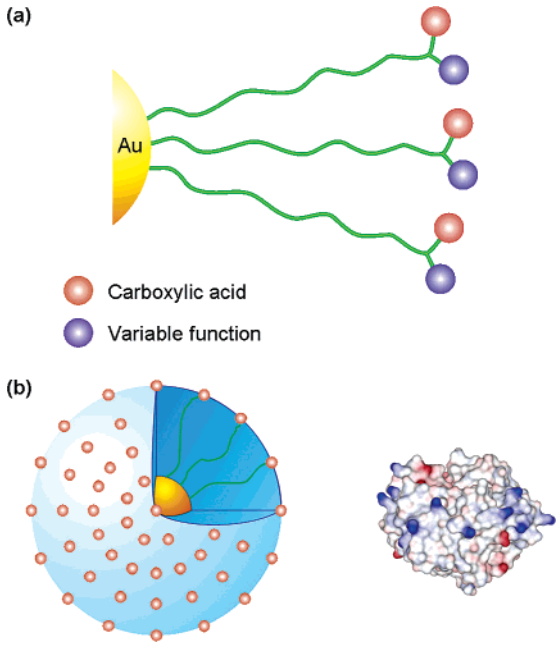

Figure 1. (a) Amino acid-decorated cluster surface that consists of carboxylic acid recognition elements as well as extra functions for perturbation. (b) The relative sizes of amino acid-functionalized gold nanoparticles and ChT. The surface of ChT is patterned with the electrostatic surface potential, showing basic and acidic domains on protein surface.

Results and Discussion

Fabrication of Amino Acid-Functionalized Gold Nanoparticles. In the past decade, ω-functionalized *n*-alkanethiols have been extensively used as building blocks in self-assembled monolayers on gold.[19] While a number of oligopeptide-functionalized thioligands have been designed and synthesized,[20] amino acid-terminated thiol ligands have rarely been reported,[21] although the latter provides more fundamental information on the monolayer construction. For example, variation in amino acid side chain structure will allow us to probe the effect of hydrophobic groups (e.g., Leu, Val), additional anionic functionality (e.g., Asp, Glu), cationic groups (e.g., Arg), and hydrogen-bonding functionality (e.g., Asn, Gln).

We have shown that carboxylate-functionalized nanoparticle clusters bind ChT and inhibit its activity through complementary electrostatic interaction.[17] In further studies, it has been revealed that tetra(ethylene glycol) tethers in the nanoparticles minimize

(13) (a) Stavens, K. B.; Pusztay, S. V.; Zou, S. H.; Andres, R. P.; Wei, A. *Langmuir* **1999**, *15*, 8337−8339. (b) Hostetler, M. J.; Wingate, J. E.; Zhong, C.-J.; Harris, J. E.; Vachet, R. W.; Clark, M. R.; Londono, J. D.; Green, S. J.; Stokes, J. J.; Wignall, G. D.; Glish, G. L.; Porter, M. D.; Evans, N. D.; Murray, R. W. *Langmuir* **1998**, *14*, 17−30.
(14) (a) Li, X.-M.; Huskens, J.; Reinhoudt, D. N. *J. Mater. Chem.* **2004**, *14*, 2954−2971. (b) Templeton, A. C.; Wuelfing, M. P.; Murray, R. W. *Acc. Chem. Res.* **2000**, *33*, 27−36.
(15) For some recent reviews, see: (a) Verma, A.; Rotello, V. M. *Chem. Commun.* **2005**, 303−312. (b) Daniel, M.-C.; Astruc, D. *Chem. Rev.* **2004**, *104*, 293−346. (c) Pasquato, L.; Pengo, P.; Scrimin, P. *J. Mater. Chem.* **2004**, *14*, 3481−3487. (d) Katz, E.; Willner, I. *Angew. Chem., Int. Ed.* **2004**, *43*, 6042−6108. (e) Shenhar R.; Rotello, V. M. *Acc. Chem. Res.* **2003**, *36*, 549−561. (f) Sastry, M.; Rao, M.; Ganesh, K. N. *Acc. Chem. Res.* **2002**, *35*, 847−855.
(16) (a) Nam, J.-M.; Stoeva, S. I.; Mirkin, C. A. *J. Am. Chem. Soc.* **2004**, *126*, 5932−5933. (b) Verma, A.; Nakade, H.; Simard, J. M.; Rotello, V. M. *J. Am. Chem. Soc.* **2004**, *126*, 10806−10807. (c) Zheng, M.; Huang, X. *J. Am. Chem. Soc.* **2004**, *126*, 12047−12054. (d) Raschke, G.; Kowarik, S.; Franzl, T.; Sönnichsen, C.; Klar, T. A.; Feldmann, J.; Nichtl, A.; Kürzinger, K. *Nano Lett.* **2003**, *3*, 935−938. (e) Wilson, R. *Chem. Commun.* **2003**, 108−109. (f) Wang, G.; Zhang, J.; Murray, R. W. *Anal. Chem.* **2002**, *74*, 4320−4327. (g) Cao, Y. C.; Jin, R.; Mirkin, C. A. *Science* **2002**, *297*, 1536−1540. (h) McIntosh, C. M.; Esposito, E. A.; Boal, A. K.; Simard, J. M.; Martin, C. T.; Rotello, V. M. *J. Am. Chem. Soc.* **2001**, *123*, 7626−7629. (i) Nath, N.; Chilkoti, A. *J. Am. Chem. Soc.* **2001**, *123*, 8197−8202.
(17) (a) Hong, R.; Emrick, T.; Rotello, V. M. *J. Am. Chem. Soc.* **2004**, *126*, 13572−12573. (b) Hong, R.; Fischer, N. O.; Verma, A.; Goodman, C. M.; Emrick, T.; Rotello, V. M. *J. Am. Chem. Soc.* **2004**, *126*, 739−743. (c) Fischer, N. O.; Verma, A.; Goodman, C. M.; Simard, J. M.; Rotello, V. M. *J. Am. Chem. Soc.* **2003**, *125*, 13387−13391. (d) Fischer, N. O.; McIntosh, C. M.; Simard, J. M.; Rotello, V. M. *Proc. Natl. Acad. Sci. U.S.A.* **2002**, *99*, 5018−5023.
(18) Coppola, G. M.; Schuster, H. F. *Asymmetric Synthesis. Construction of Chiral Molecules Using Amino Acids*; Wiley: New York, 1987.
(19) Witt, D.; Klajn, R.; Barski, P.; Grzybowski, B. A. *Curr. Org. Chem.* **2004**, *8*, 1763−1797.
(20) (a) Pengo, P.; Polizzi, S.; Pasquato, L.; Scrimin, P. *J. Am. Chem. Soc.* **2005**, *127*, 1616−1617. (b) Pengo, P.; Broxterman, Q. B.; Kaptein, B.; Pasquato, L.; Scrimin, P. *Langmuir* **2003**, *19*, 2521−2524. (c) Templeton, A. C.; Hostetler, M. J.; Warmoth, E. K.; Chen, S.; Hartshorn, C. M.; Krishnamurthy, V. M.; Forbes, M. D. E.; Murray, R. W. *J. Am. Chem. Soc.* **1998**, *120*, 4845−4849. (d) Schaaff, T. G.; Knight, G.; Shafigullin, M. N.; Borkman, R. F.; Whetten, R. L. *J. Phys. Chem. B* **1998**, *102*, 10643−10646. (e) Roberts, C.; Chen, C. S.; Mrksich, M.; Martichonok, V.; Ingber, D. E.; Whitesides, G. M. *J. Am. Chem. Soc.* **1998**, *120*, 6548−6555.
(21) Nissink, J. W. M.; Maas, J. H. *Appl. Spectrosc.* **1999**, *53*, 33−39.

Scheme 1. Synthesis of L-Amino Acid-Terminated Thiol Ligands

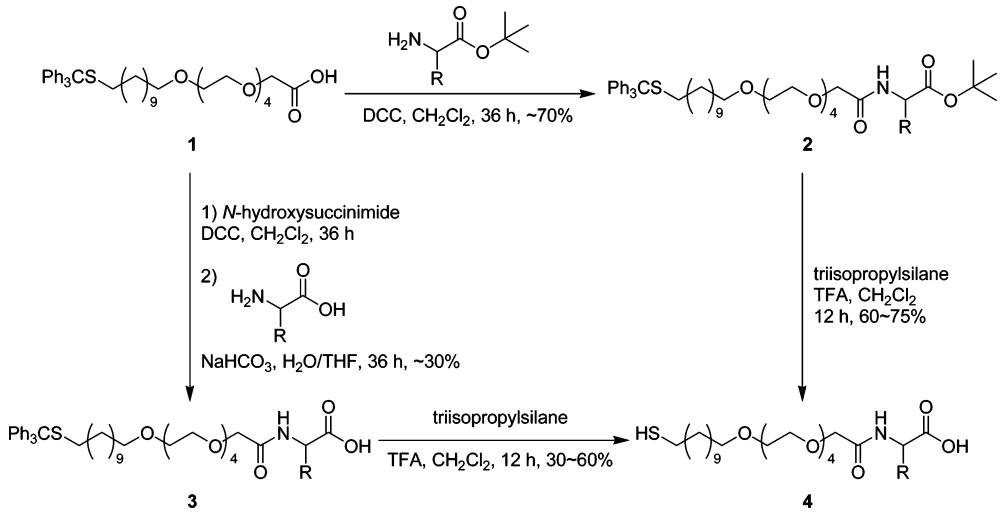

Scheme 2. Fabrication of L-Amino Acid-Functionalized Gold Nanoparticles through Place-Exchange Reaction

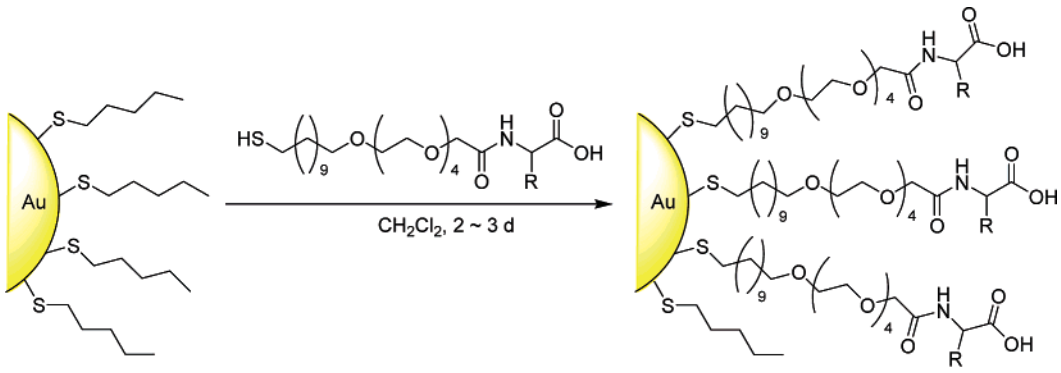

NP_Gly: R = -H
NP_L-Ala: R = $-CH_3$
NP_L-Arg: R = $-CH_2CH_2CH_2NHC(NH)NH_2$
NP_L-Asn: R = $-CH_2CONH_2$
NP_L-Asp: R = $-CH_2COOH$
NP_L-Gln: R = $-CH_2CH_2CONH_2$
NP_L-Glu: R = $-CH_2CH_2COOH$
NP_L-Leu: R = $-CH_2CH(CH_3)_2$
NP_L-Met: R = $-CH_2CH_2SCH_3$
NP_L-Phe: R = $-CH_2C_6H_5$
NP_L-Val: R = $-CH(CH_3)_2$

the nonspecific protein adsorption and preserve the secondary structure of adsorbed protein.[17b,22] In this context, trityl protected 26-mercapto-3,6,9,12,15-pentaoxahexacosan-1-oic acid **1** was prepared according to Houseman and Mrksich's protocol[23] and was used as the starting compound for the preparation of amino acid-functionalized thiol ligands. As shown in Scheme 1, two methods have been employed to incorporate amino acids into the thiol ligands. In one method, target thiol ligands **4** were synthesized by the reaction of **1** with L-amino acid *tert*-butyl esters in dry dichloromethane through the activation of carboxylic acid function by dicyclohexylcarbodiimide (DCC), followed by removal of trityl and *tert*-butyl groups in trifluoroacetic acid (TFA) with triisopropylsilane as a hydride donor.[24] Alternatively, the coupling reaction of **1** with *N*-hydroxysuccinimide afforded corresponding active ester, which was further reacted with free L-amino acids in a mixed solvent of THF and H_2O and successively treated with TFA to give the amino acid ligands **4** (see Supporting Information).

Once the amino acid-functionalized alkanethiols were obtained, they were subjected to ligand exchange reaction[25] with 1-pentanethiol-coated gold nanoparticle (**C_5-NP**, $d \approx 2.0$ nm).[26] While **C_5-NP** is highly soluble in dichloromethane, the ligand exchanged nanoparticles were fully precipitated from the solution. Thus, the nanoparticles were conveniently collected by centrifugation. All of the resultant nanoparticles show good solubility in water. Scheme 2 illustrates the fabrication of amino acid-decorated gold nanoparticles and their structures. In ^{1}H NMR spectra of the nanoparticles, no signals from the methyl groups in C_5 ligands are observed, indicating that the ligand exchange is achieved essentially quantitatively. As Murray and co-workers' research has demonstrated that place-exchange proceeds in a 1:1 stoichiometry,[25] ~100 amino acid ligands are estimated to be present on our 2 nm core particles.[25]

(22) (a) Zheng, M.; Davidson, F.; Huang, X. *J. Am. Chem. Soc.* **2003**, *125*, 7790−7791. (b) Herrwerth, S.; Eck, W.; Reinhardt, S.; Grunze, M. *J. Am. Chem. Soc.* **2003**, *125*, 9359−9366. (c) Kane, R. S.; Deschatelets, P.; Whitesides, G. M. *Langmuir* **2003**, *19*, 2388−2391. (d) Harris, J. M., Ed. *Poly(ethylene Glycol) Chemistry: Biotechnical and Biomedical Applications*; Plenum Press: New York, 1992.
(23) Houseman, B. T.; Mrksich, M. *J. Org. Chem.* **1998**, *63*, 7552−7555.
(24) Greene, T. W.; Wuts, P. G. M. *Protective Groups in Organic Synthesis*, 3rd ed.; John Wiley & Sons: New York, 1999.
(25) (a) Hostetler, M. J.; Templeton, A. C.; Murray, R. W. *Langmuir* **1999**, *15*, 3782−3789. (b) Hostetler, M. J.; Green, S. J.; Stokes, J. J.; Murray, R. W. *J. Am. Chem. Soc.* **1996**, *118*, 4212−4213.
(26) Brust, M.; Walker, M.; Bethell, D.; Schiffrin, D. J.; Whyman, R. *J. Chem. Soc., Chem. Commun.* **1994**, 801−802.

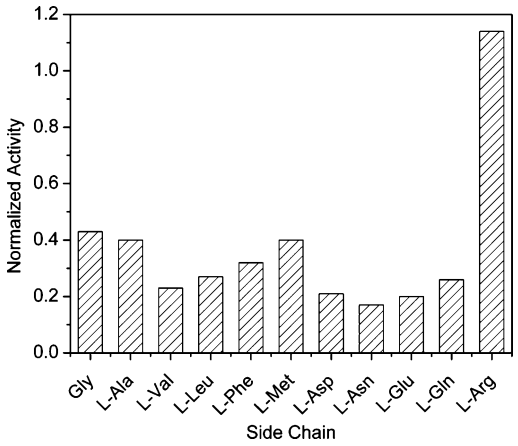

Figure 2. Normalized activity of ChT (3.2 μM) with nanoparticles (0.8 μM) bearing various amino acid side chains.

ChT Activity Assays and Binding Affinity. Because the ChT active site is surrounded by cationic residues, negatively charged nanoparticles can block the active site and subsequently diminish the accessibility of negatively charged substrates to the catalytic center, resulting in the inhibition of ChT activity.[17] To probe the interaction between ChT and the amino acid-terminated gold nanoparticles, the ChT-catalyzed hydrolysis of *N*-succinyl-L-phenylalanine *p*-nitroanilide (SPNA) was first examined in the presence of various concentrations of nanoparticles. The activities of ChT in the presence of nanoparticles were normalized to that of free ChT.

The results show that the nanoparticles exhibit quite a different influence on the activity of ChT. For most amino acid-decorated gold nanoparticles, the rate of ChT-catalyzed hydrolysis of SPNA decreased upon addition of nanoparticles, clearly suggesting the activity inhibition through complex formation (Figure 2). The only exception is L-Arg-terminated gold nanoparticle, where slight superactivity of ChT was observed in the presence of **NP_L-Arg**, indicating that no significant interaction exists between ChT and **NP_L-Arg**.[17d] Circular dichroism and fluorescence studies gave the same conclusion (vide post). All of the other hydrophobic, neutral polar, or negatively charged amino acids-decorated gold nanoparticles show considerable inhibition of ChT activity, indicating that the complementary electrostatic interaction is essential for the formation of ChT−NP complexes.

From Figure 2, it is apparent that inhibition of ChT activity depends critically on the side chain properties of nanoparticles. While no inhibition effect was observed for **NP_L-Arg**, the nanoparticles with polar side chains, for example, **NP_L-Asp**, **NP_L-Asn**, and **NP_L-Glu**, showed the strongest inhibitory potency with around 80% ChT activity suppression, while the nanoparticles with hydrophobic side chains exhibited less pronounced inhibition. **NP_L-Met** and **NP_L-Ala**, for instance, showed only 60% inhibition on ChT activity. This observation can be attributed to the hydrophobicity difference of ChT active site in the presence of different nanoparticles. Presumably, the hydrophobic active site of ChT is more accessible by SPNA in comparison with that surrounded by nanoparticles bearing polar side chains, because the hydrophobic phenylalanine residue in the substrate needs first to be bound into the active site during the enzyme-promoted cleavage of peptide bonds.[17a] As a consequence, more residual activity of ChT was detected for the interaction with nanoparticles carrying hydrophobic side chains.

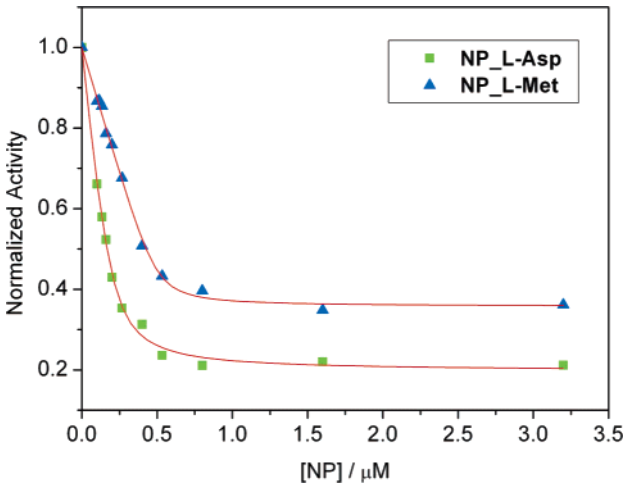

Figure 3. Nonlinear least-squares curve-fitting analysis of the activity assay data ([ChT] = 3.2 μM).

Table 1. Microscopic Binding Constant (K_S), Gibbs Free Energy Change ($-\Delta G$), and Binding Ratio (n) for the Complexation of ChT with Nanoparticles in Phosphate Buffer (5 mM, pH 7.4) at 30 °C[a]

nanoparticle	$K_S/10^6$ M^{-1}	$-\Delta G$/kJ mol^{-1}	n
NP_Gly	2.9	37.5	7.3 ± 1.5
NP_L-Ala	7.8	40.0	6.2 ± 0.2
NP_L-Asn	2.7	37.3	6.7 ± 0.9
NP_L-Asp	2.2	36.8	13.1 ± 0.3
NP_L-Gln	3.0	37.6	6.8 ± 0.5
NP_L-Glu	2.4	37.0	9.1 ± 0.7
NP_L-Leu	5.9	39.3	6.4 ± 0.4
NP_L-Met	13.1	41.3	6.4 ± 0.2
NP_L-Phe	7.1	39.8	6.8 ± 0.7
NP_L-Val	8.1	40.1	7.6 ± 0.2

[a] The error of binding constants was usually less than 20%. The magnitude of binding strength was further confirmed by fluorescence titration study on the system of ChT and **NP_L-Leu**, which gave a binding constant of 5.3×10^6 M^{-1} (see Supporting Information).

The activity assay results were further analyzed to evaluate the association strength between ChT and nanoparticles. Assuming that nanoparticles have a number of identical and independent binding sites (i.e., n) that could bind a ChT molecule each, the microscopic binding constants (K_S) and binding ratios (n) can be simultaneously estimated by using nonlinear least-squares curve-fitting analysis on the data of activity assays (see Supporting Information). Representative fitting curves are shown in Figure 3, in which no serious deviations are observed. The excellent curve fits indicate the reliability of the stability constants. The binding constants and binding ratios are summarized in Table 1.

From Table 1, it can be seen that the binding constants are also dependent on the side chains of the nanoparticles. For nanoparticles with hydrophilic amino acid side chains, that is, **NP_L-Asp**, **NP_L-Glu**, **NP_L-Asn**, and **NP_L-Gln**, the binding constants are around 3×10^6 M^{-1}, comparable to that of **NP_Gly**. For nanoparticles with hydrophobic amino acid side chains, considerably enhanced binding affinity is observed. For **NP_L-Met**, the highest binding constant of 1.3×10^7 M^{-1} is obtained, which is 4 times that for reference nanoparticle **NP_Gly**. These results expressly indicate that the hydrophobic side chain aids the interaction between nanoparticles and ChT. A plot of the Gibbs free energy changes ($-\Delta G$) for the

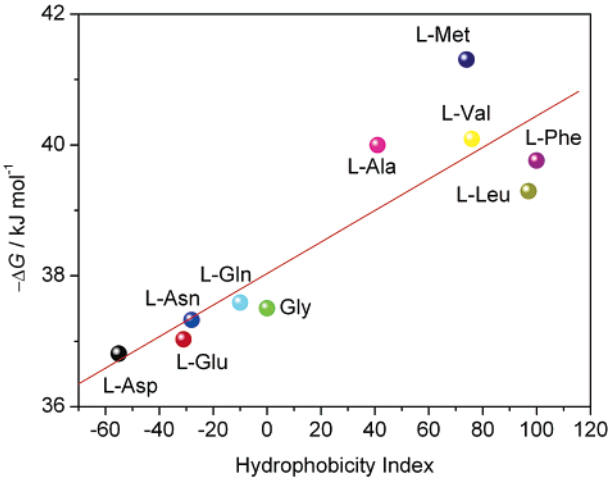

Figure 4. Correlation between Gibbs free energy changes and hydrophobicity index of amino acid side chains; represents linear fit of the data.

complexation of ChT with various nanoparticles versus the hydrophobicity index[27] of amino acid side chains shows the correlation between the binding strength and hydrophobicity of the side chains (Figure 4).

Gel Electrophoresis and Binding Ratio. It should be noted from Table 1 that most nanoparticles have binding stoichiometries as determined through activity assays of ∼7, except for **NP_**L-**Asp** and **NP_**L-**Glu** that have considerably higher values of 13 and 9, respectively. To confirm the binding ratios, gel electrophoresis with various ChT/NP ratios was performed. As can be seen from Figure 5, the gel electrophoresis results unambiguously supported the formation of ChT−NP complexes through charge complementarity. The pre-stain and post-stain in Figure 5 refer to the treatment of gels before and after staining of the protein with Comassie Blue, allowing us to observe the brown nanoparticles before staining and visualize the protein post-staining. The narrow bands observed for the ChT−NP complex suggest the formation of discrete complexes rather than extended ChT−NP aggregates. The maximum positive movement for the particle in the pre-stained gel provides a means for estimating binding stoichiometries. These studies indicate that the binding stoichiometry of **NP_**L-**Asn** and ChT is 1:7, while the value for **NP_**L-**Asp** and ChT is 1:12. These results agree well with the corresponding values elucidated from the activity assays. The gel electrophoresis studies on the other nanoparticle/ChT systems also gave results consistent with activity assays, with binding stoichiometries for monotopic amino acid-functionalized nanoparticles around 1:7, while the value for **NP_**L-**Glu** was 1:10.

Our previous study revealed that complete inhibition of ChT using 11-mercaptoundencanoic acid capped gold nanoparticle (**NP_MUA**, $d = 5.5$ nm) could be accomplished at a NP:ChT binding ratio of 1:4.[17c,d] Molecular modeling showed that the dimension of amino acid-functionalized thiol ligands is around 4 nm, so that the diameters of current nanoparticles are significantly larger than **NP_MUA** by 4.5 nm (2 nm Au core + ∼8 nm for the ligand chain). Therefore, it is estimated that the surface area of the current nanoparticles increases ca. 3-fold

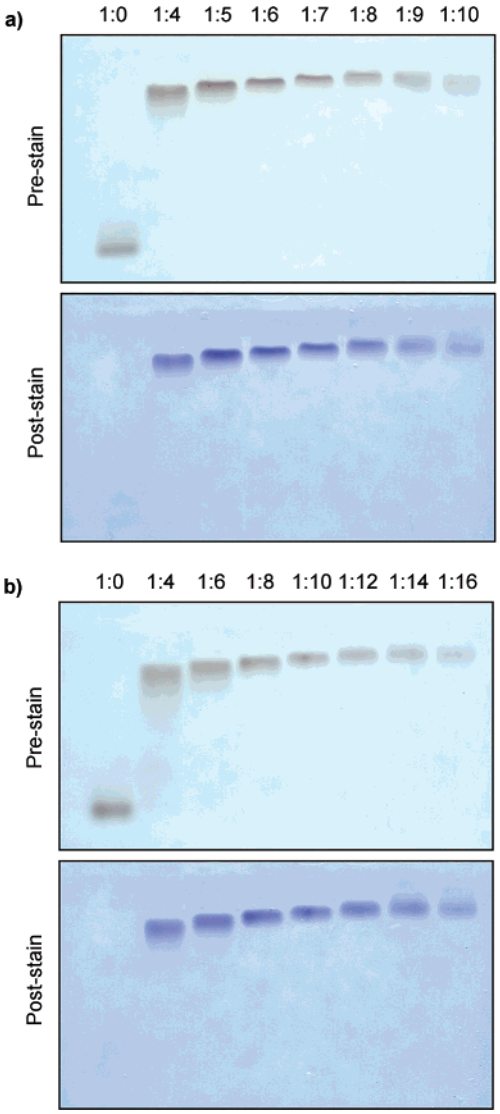

Figure 5. Gel electrophoresis of ChT and **NP_**L-**Asn** (a) and **NP_**L-**Asp** (b). Nanoparticle concentrations were varied at a constant ChT concentration (50 μM).

in comparison with **NP_MUA** by assuming regular spherical topology. If the binding stoichiometry is critically dependent on the area of nanoparticle surface, then all of the nanoparticles should have a binding ratio of 1:12 based on complete coverage of the nanoparticle surface by ChT. This is not the case, suggesting that except for **NP_**L-**Asp** and **NP_**L-**Glu** the nanoparticle surface is not fully saturated. From the viewpoints of structure, the number of carboxylates in ditopic amino acid-functionalized nanoparticles (e.g., **NP_**L-**Asp**) should be twice that of monotopic amino acid-functionalized nanoparticles (e.g., **NP_**L-**Asn**) if they have the same number of ligands on the gold core. Thus, it seems that the surface charge density also affects the binding ratio. X-ray single crystal analysis revealed that 12 positively charged residues (L-Lys and L-Arg) are located on the same side of ChT surface and surround the active site (Figure 1),[28] which can take part in the electrostatic interaction with nanoparticles. On the other hand, it has been demonstrated that roughly 100 ligands are attached to the Au core in 2 nm

(27) Monera, O. D.; Sereda, T. J.; Zhou, N. E.; Kay, C. M.; Hodges, R. S. *J. Pept. Sci.* **1995**, *1*, 319−329. This hydrophobicity index is normalized so that the most hydrophobic residue (L-Phe) is given a value of 100 relative to glycine, which is considered neutral (value 0). The scales are extrapolated to residues that are more hydrophilic than glycine.

(28) (a) Tsukada, H.; Blow, D. M. *J. Mol. Biol.* **1985**, *184*, 703−711. (b) Blow, D. M. *Acc. Chem. Res.* **1976**, *9*, 145−152.

Table 2. Zeta-Potentials for Various Amino Acid-Functionalized Gold Nanoparticles in PBS Buffer (20 mM potassium phosphate and 100 mM sodium chloride, pH 7.8) at 25.0 °C

nanoparticle	zeta-potential/mV	nanoparticle	zeta-potential/mV
NP_Gly	−25.8 ± 1.5	**NP_L-Glu**	−32.2 ± 0.7
NP_L-Ala	−24.7 ± 2.1	**NP_L-Leu**	−25.6 ± 1.5
NP_L-Asn	−26.2 ± 0.5	**NP_L-Met**	−25.4 ± 2.0
NP_L-Asp	−32.5 ± 0.4	**NP_L-Phe**	−25.7 ± 1.8
NP_L-Gln	−23.5 ± 1.2	**NP_L-Val**	−26.4 ± 1.6

gold nanoparticles.[25] Therefore, if the electrostatic interaction takes place in a 1:1 negative/positive charge ratio or ion pair form, **NP_L-Asn** might bind 8 ChT molecules, while **NP_L-Asp** has the capacity of associating 16 ChT molecules. These values are quite close to the observed binding stoichiometries, suggesting that complete charge pairing is a prerequisite for efficient binding.

As place-exchange proceeds in a 1:1 stoichiometry[25] and we have complete (by NMR) exchange of the C5 ligands, the charge on the ditopic particles (i.e., **NP_L-Asp** and **NP_L-Asp**) is expected to be twice that of the monotopic analogues. Qualitative evidence of this expected surface charge disparity of these nanoparticles was obtained by measuring the zeta-potentials of particles in PBS buffer at 25.0 °C (Table 2.) As can be seen, all monotopic amino acid-functionalized nanoparticles have zeta-potentials of about −25 mV, while the ditopic amino acid-functionalized nanoparticles such as **NP_L-Asp** and **NP_L-Glu** afford zeta-potentials of around −32 mV. Although the relationship between zeta-potential and charge is not straightforward due to the complex relationship between surface structure and measured values,[29] these results indicate that the nanoparticles bearing ditopic amino acid functions possess more negatively charged surfaces.

In this context, one rational explanation for the binding ratio difference between mono- and ditopic amino acid-functionalized nanoparticles is that the flexible nanoparticle surfaces would adopt allosteric conformations to achieve the maximal amount of electrostatic interactions during the complexation process (Figure 6). Consequently, the surface of nanoparticles with monotopic amino acids is less saturated than that of **NP_L-Asp** or **NP_L-Glu** by the protein, because the formers have fewer recognition elements (i.e., carboxylates) on the surface. The charge-complementary interaction between ChT and NP is therefore not only dependent on the relative surface areas, but also regard to the number of charged "hot spots".

Circular Dichroism. Another important issue to be addressed is the influence of amino acid side chains on the conformation of ChT. No CD signals are detected from the nanoparticles, indicating that the amino acids on the surface are not organized to an ordered assembly. Figure 7 illustrates the CD spectra of ChT and ChT with different nanoparticles after 24 h incubation. It is significant that the CD spectra of ChT are drastically dependent upon the amino acid side chains of nanoparticles. While almost no change in the CD spectrum of ChT was observed with **NP_L-Leu**, nanoparticles with L-Asn and L-Asp side chains induced varying levels of CD spectral changes of ChT, that is, the diminishing of the characteristic minimum at 232 nm and the hypochromic shift of the minimum at 204 nm. Systematic study showed that the CD signals of ChT are little

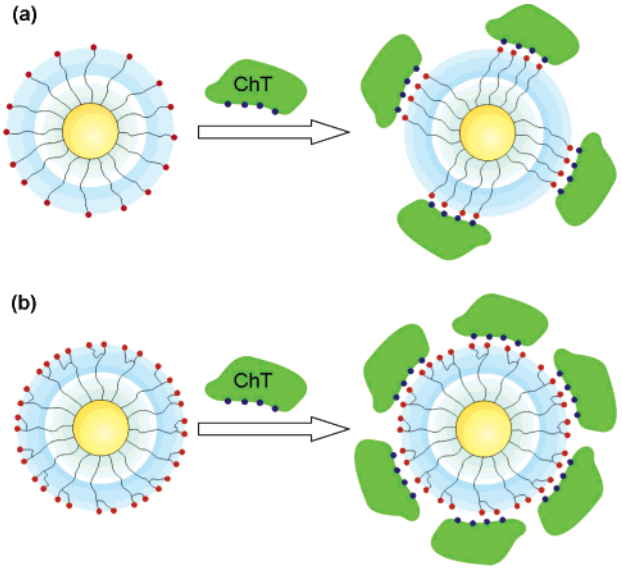

Figure 6. Schematic illustration for the binding modes of ChT with nanoparticles bearing (a) monotopic and (b) ditopic amino acid functions. In the former case, the surface carboxylate functions are proposed to reorganize to maximize the electrostatic interactions.

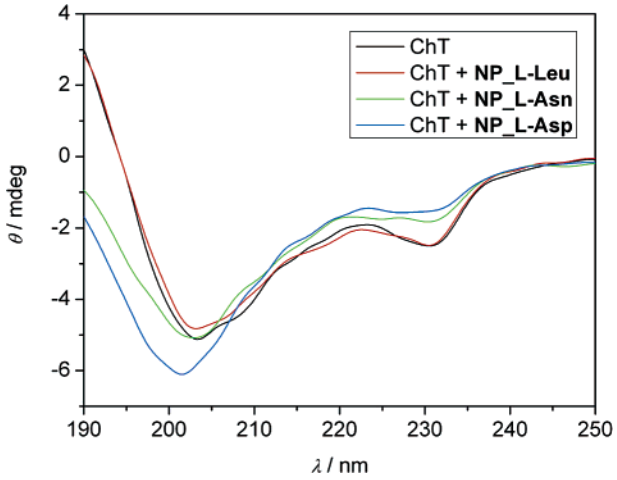

Figure 7. Circular dichroism spectra of ChT (3.2 μM) and ChT with nanoparticles (0.8 μM) after 24 h incubation. The weak CD signal of the nanoparticles has been subtracted from that of the complex.

influenced by the presence of nanoparticles bearing hydrophobic amino acid side chains such as **NP_L-Phe**, **NP_L-Leu**, **NP_L-Met**, **NP_L-Val**, and **NP_L-Ala**, while ChT experiences conformational changes in the presence of nanoparticles bearing polar amino acid side chains, for example, **NP_Gly**, **NP_L-Gln**, **NP_L-Asn**, **NP_L-Glu**, and **NP_L-Asp**. The spectral changes were time-dependent, suggesting that the polar amino acid side chains induced the conformational changes of ChT, whereas the hydrophobic amino acid side chains had little effect on ChT structure. As expected, **NP_L-Arg** does not perturb the CD spectrum of ChT.

Fluorescence and Denaturation Kinetics. To obtain insight into the kinetics of the denaturation process of ChT in the presence of nanoparticles, the characteristic fluorescence of tryptophan residues in ChT was investigated using steady-state fluorescence spectrometry, which is more sensitive than CD. As shown in Figure 8, the intrinsic emission of ChT shows a maximum at 331 nm in buffer solution. However, significant bathochromic shifts and peak broadening were observed after

(29) Kirby, B. J.; Hasselbrink, E. F., Jr. *Electrophoresis* **2004**, *25*, 187−202.

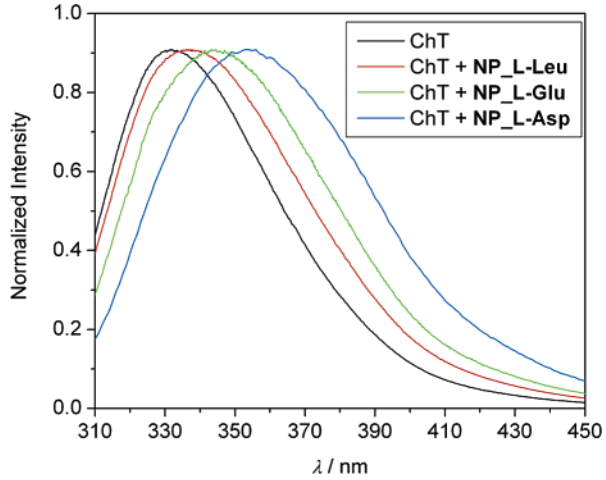

Figure 8. Fluorescence spectra of ChT (3.2 μM) and ChT with nanoparticles (0.8 μM) after 24 h incubation.

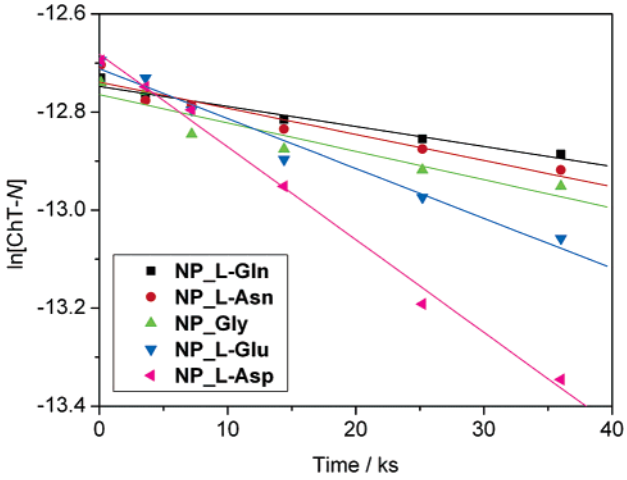

Figure 9. Linear plots for the first-order chymotrypsin denaturation in the presence of different nanoparticles in 5 mM sodium phosphate buffer (pH 7.4). The amount of native α-chymotrypsin was calculated from the fluorescence shifts by assuming that the shifts are proportional to the denatured species.

incubation with nanoparticles for 24 h. The maximal fluorescence shift of 23 nm was observed for the ChT incubated with **NP_L-Asp**, with concomitant broadening of half-maximal amplitude from 52 to 68 nm. These phenomena indicate that the initially buried tryptophan residues were exposed to more polar environment due to the denaturation of the protein.[30] The extent of denaturation of ChT is reflected by the different values of fluorescence shift, which is again linked to the properties of amino acid side chains in nanoparticles. If we consider that the fluorescence maximum at 356 nm (i.e., L-Trp in water) corresponds to a complete denaturation of ChT, we may roughly estimate the extent of protein denaturation by nanoparticles. For example, after 24 h incubation, hydrophilic **NP_L-Asp** and **NP_L-Asn** induce ca. 90% and 40% denaturation of ChT, respectively, while hydrophobic **NP_L-Phe** and **NP_L-Leu** induce only 10% and 20% denaturation.

The denaturation of ChT should occur in a two-state process as described in eq 1:

$$\text{ChT-}N \xrightarrow{k} \text{ChT-}D \qquad (1)$$

where ChT-*N* is the native form and ChT-*D* the denatured form, and *k* denotes the rate constant. In principle, the denaturation should follow a first-order reaction profile.

In Figure 9, the logarithm of native ChT concentration was plotted against time (over a period of 10 h). Good linear regressions were found for all systems, unambiguously confirming the first-order denaturation profiles. Interestingly, the rate of ChT denaturation decreases with the increase of the hydrophobicity of amino acid side chains. The rate constants obtained by the linear regression together with the fluorescence shifts after 24 h incubation are listed in Table 3.

From Table 3, it can be seen that the denaturation rates are in accordance with the extent of final fluorescence shifts after 24 h incubation. As expected, **NP_L-Asp** induces the fast denaturation of ChT with a rate constant of 1.89×10^{-5} M^{-1} s^{-1}. For **NP_L-Asn**, the rate constant drops by two-thirds to 5.33×10^{-6} M^{-1} s^{-1}. Similarly, for the L-Glu/L-Gln counterparts, the rate constants decrease from 1.02×10^{-5} to 4.08×10^{-6} M^{-1} s^{-1}. These observations strongly suggest that the carboxylate functions facilitate the denaturation process. As pointed out previously, the competitive hydrogen-bonding formation may destabilize the α-helices in ChT and disrupt their secondary structure. Furthermore, these phenomena are most probably attributed to the fact that the salt bridge (i.e., between the *N*-terminus of Ile16 and the Asp194 side chain) in the protein is more easily broken by the charged side chains. Indeed, the observed denaturation rates for **NP_L-Asp** and **NP_L-Glu** are comparable to the denaturation rate of ChT at pH 11.0 (i.e., $k = 1.43 \times 10^{-5}$ M^{-1} s^{-1}),[31] where hydroxide ions are believed to be involved in the breakage of salt bridges.[32]

Table 3. First-Order Rate Constants for the Denaturation of ChT in the Presence of Various Nanoparticles and the Fluorescence Shifts after Incubation for 24 h

nanoparticles	$k/10^{-6}$ M^{-1} s^{-1}	$\Delta\lambda_{em}$/nm
NP_Gly	5.79	11.4
NP_L-Ala	3.73	6.2
NP_L-Asn	5.33	9.4
NP_L-Asp	18.92	23.0
NP_L-Gln	4.08	8.2
NP_L-Glu	10.18	13.4
NP_L-Leu	3.31	5.0
NP_L-Met	0.61	3.2
NP_L-Phe	0.41	2.2
NP_L-Val	3.27	5.8

In contrast to the above observations, the hydrophobic amino acid side chains induced little change in ChT secondary structure. **NP_L-Phe**, the nanoparticle bearing the most hydrophobic side chain, gives a denaturation rate constant of only 4.1×10^{-7} M^{-1} s^{-1}, decreasing by 50 times in comparison with **NP_L-Asp**. Both CD and fluorescence studies have revealed that the hydrophobicity of amino acid side chains shows impacts on the denaturation of ChT. Therefore, the denaturation rate constants of ChT in diverse nanoparticles were again plotted against the hydrophobicity index[27] of amino acid side chains in Figure 10. This plot shows that the dianionic side chains strongly increase the rate of denaturation. The other side chains show a

(30) Ladokhin, A. S. In *Encyclopedia of Analytical Chemistry*; Meyers, R. A., Ed.; John Wiley & Sons Ltd.: Chichester, U.K., 2000; pp 5762−5779.
(31) Wu, H.-L.; Lace, D. A.; Bender, M. L. *Proc. Natl. Acad. Sci. U.S.A.* **1981**, *78*, 4118−4119.
(32) Wroblowski, B.; Díaz, J. F.; Schlitter, J.; Engelborghs, Y. *Protein Eng.* **1997**, *10*, 1163−1174.

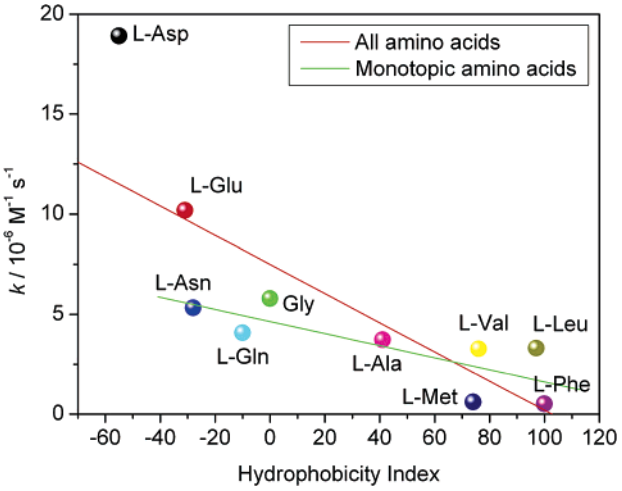

Figure 10. Correlation between the denaturation rate constants (k) of ChT and the hydrophobicity index of amino acid side chains in nanoparticles.

lesser but still evident correlation between hydrophobicity and denaturation rate, indicating that the hydrophobicity of amino acid side chains in nanoparticles plays a role in ChT denaturation/stabilization.

Our previous study has shown that the alkyl interior in **NP_MUA** induces the drastic denaturation of ChT,[17c,d] whereas the current hydrophobic amino acid side has little effect on the native structure of the bound ChT. One plausible interpretation for these phenomena is that in the former case the alkyl chain nonspecifically interacts with the whole surface of ChT and therefore destabilizes the protein. In the latter, however, the hydrophobic amino acid side chains exclusively interact with the hydrophobic patches on the ChT surface and preserve the protein structure much as in the natural protein−protein interaction. Indeed, selective introduction of hydrophobic groups near the hydrophobic region on protein surface has proven to be one method of choice for improving protein stabilization.[33]

Conclusions

In summary, we have demonstrated that the functionality of monolayer protected gold nanoparticles could be readily tailored by introducing diverse terminal functions. By incorporating simple L-amino acids, nanoparticles exhibit distinctly different inhibition ability on ChT activity. Complementary electrostatic interaction between nanoparticles and ChT was proven to be the predominant driving force contributing to the complex formation, but the hydrophobic interaction between the hydrophobic patches of receptors and proteins enhanced the complex stability. The binding capacity of these receptors depends not only on the surface areas of nanoparticles, but also on their surface charge density. Additionally, the hydrophobicity of amino acid side chains shows great influence on the secondary structure of ChT. The hydrophobic side chains have little effect on ChT structure, while the hydrophilic side chains destabilize the protein. Taken together, the control over association/dissociation as well as stabilization/denaturation of ChT at the MMPC interfaces has been conveniently accomplished by introducing additional functions in the vicinity of carboxylic acid functions. These fundamental insights into the interaction between proteins and artificial receptors with nanoparticle scaffolds offer opportunities for developing novel core/shell receptors with highly specific protein-surface recognition ability, which would possess promising applications in protein stabilization, alteration, and delivery.

Experimental Section

General. α-Chymotrypsin (type II from bovine pancreas, ChT), *N*-succinyl-L-phenylalanine *p*-nitroanilide (SPNA), and *tert*-butyl esters of amino acids (Gly, L-Phe, L-Ala, L-Val, L-Leu, L-Met, and L-Glu) were purchased from Sigma and used as received. All of the other chemicals were obtained from Aldrich unless otherwise stated. The solvents used for chemical synthesis were purified and dried according to standard procedures.[34] Trityl protected acid **1** was prepared according to the procedure described by Houseman and Mrksich.[23] Subsequently, trityl protected acid **1** was reacted either with *tert*-butyl esters of amino acids or successively with *N*-hydroxysuccinimide and free amino acids, followed by the treatment with trifluoroacetic acid and triisopropylsilane, affording corresponding mercaptoligands bearing amino acid terminals. The purification of all intermediates and ligands was performed on flash chromatography (SiO_2, particle size 0.032−063 mm). Pentanethiol capped gold nanoparticle ($d \approx 2$ nm) was prepared according to the reported method.[26] Ligand exchange in dichloromethane was carried out to produce amino acid-decorated gold nanoparticles (NPs).[25] The reaction details and the characterization of products were compiled in the Supporting Information.

Activity Assays. All of the experiments were performed in sodium phosphate buffer (5 mM, pH 7.4) with [ChT] = 3.2 μM and variant NP concentrations. The enzymatic hydrolysis reaction was initiated by adding a SPNA stock solution (16 μL) in ethanol to a preincubated ChT−NP solution (184 μL) to reach a final SPNA concentration of 2 mM. Enzyme activity was followed by monitoring product formation every 15 s for 15 min at 405 nm with a microplate reader (EL808IU, Bio-Tek Instruments, Winooski, VT). Control experiment showed that the autohydrolysis of SPNA was negligible during the time course of activity assay. The assays were performed in duplicates or triplicates, and the averages are reported. The standard deviation was usually less than 10%.

Gel Electrophoresis. Agarose gels were prepared in 5 mM sodium phosphate buffer at 1% final agarose concentration. Appropriately sized wells (40 μL) were generated by placing a comb in the center of the gel. A ChT stock solution of 100 μM in 5 mM sodium phosphate buffer (pH 7.4) was used to prepare 30 μL samples at the appropriate ChT/NP ratios ([ChT] = 50 mM). After a 30 min incubation period at room temperature, 3 μL of 80% glycerol was added to ensure proper well loading (30 μL), and a constant voltage (100 V) was applied for 30 min for sufficient separation. Gels were placed in staining solution (0.5% Coomassie blue, 40% methanol, 10% acetic acid aqueous solution) for 1 h, followed by extensive destaining (40% methanol, 10% acetic acid aqueous solution) until protein bands were clear. Gels were scanned on a flatbed scanner both prior to and after staining to separately visualize particle and ChT bands.

Zeta-Potential. Amino acid-functionalized gold nanoparticles were dissolved in PBS buffer (20 mM potassium phosphate and 100 mM sodium chloride, pH 7.8) to make a 1 μM solution, and their zeta-potentials were measured on a MALVERN Zetasizer Nano ZS instrument. Three rounds of assays have been performed, and the average values were reported.

Circular Dichroism. Far-UV circular dichroism (CD) spectra of ChT (3.2 μM) were measured on a JASCO J-720 spectropolarimeter with quartz cuvettes of 1 mm path length at 20 °C. The spectra were recorded from 190 to 250 nm as an average of three scans at a rate of 20 nm/min. The concentration of NPs is 0.8 μM, and their CD spectra were subtracted to eliminate background effects.

(33) Chotia, C. *Annu. Rev. Biochem.* **1984**, *53*, 537−572.

(34) Perrin, D. D.; Armarego, W. L. F. *Purification of Laboratory Chemicals*, 3rd ed.; Pergamon Press: Oxford, 1988.

Fluorescence. Fluorescence spectra were measured in a conventional quartz cuvette (10 × 10 × 40 mm) on a Shimadzu RF-5301 PC spectrofluorophotometer at room temperature (ca. 20 °C). The samples were excited at 295 nm, and the emission spectra were recorded from 300 to 450 nm. For the denaturation study, the sample concentrations are the same as those in the CD study.

Acknowledgment. This research was supported by the National Institutes of Health (GM 59249).

Supporting Information Available: Synthesis and characterization of compounds **2**, **3**, and **4**, ^{1}H NMR spectra of nanoparticles, and the algorithm for the estimation of binding constants from activity assays. This material is available free of charge via the Internet at http://pubs.acs.org.

JA0512881